ARTICLE NO. 79-1511R

J80-118

Careful Numerical Study of Flowfields about Symmetric External Conical Corners

20005
20017
20018

Manuel D. Salas*
NASA Langley Research Center, Hampton, Va.

A numerical study of the flowfield about symmetrical external axial corners formed by the juncture of swept compressive wedges is presented. The geometrical configuration under investigation allows a unified treatment of external corners typical of delta wings and of rectangular inlets. Comparisons are made with other numerical results. For the delta wing configuration, the occurrence of an anomalous shock behavior predicted by Gonor is refuted. A parametric study shows the singular behavior of the pressure at the corner as a function of the external corner angle, and a second parametric study shows the effect of the corner radius on the location of the crossflow stagnation point. Previous theoretical predictions of certain flow features typical of corner flows agree well with present numerical results.

I. Introduction

THE external corner configuration considered in this paper is formed by the intersection of two compression wedges. One of these wedges rests on the horizontal x,z plane (Fig. 1) and is defined in terms of a compression angle δ_1 and a leading-edge sweep angle Λ_1. The other wedge rests on a plane which is Ω degrees clockwise from the vertical y,z plane and is also defined in terms of a compression angle δ_2 and a leading-edge sweep angle Λ_2. In this paper we will consider only the symmetric flows† which result when the defining angles of the two wedges are equal, $\Lambda=\Lambda_1=\Lambda_2$, $\delta=\delta_1=\delta_2$, and the free stream is uniform and aligned with the symmetry plane. In addition, we restrict the values of δ and Λ to those combinations for which a critical Mach number M_* exists, such that for freestream Mach numbers greater than M_* a shock attached to the leading edges is formed (Fig. 2). Furthermore, since the wedges are assumed to be infinite in extent, no characteristic length can be defined, and the inviscid supersonic flow field to be considered is conically self-similar with the conical origin at point 0 of Fig. 1. The purpose of this paper is to present a comprehensive, unified, numerical study of this conical flowfield.

Various geometrical arrangements are possible through variations of the angle Ω. Of particular interest is the delta wing configuration which results when Ω is a right angle. This configuration has been the subject of intensive study in terms of linear theory[1] and in terms of thin-shock-layer theory.[2,3] The results of the thin-shock-layer theory are interesting in that an anomalous shock behavior is predicted at certain angles of attack. This problem will be discussed in some detail in Sec. IV.

A second aerodynamically important configuration is obtained when Ω is zero. This configuration is typical of geometric features, such as rectangular inlets, found on high-speed aircraft. The linear problem for this configuration was studied in Ref. 4, and solutions to the nonlinear problem were first presented in Ref. 5, and later in more detail in Ref. 6. Two significant features which had already been found in the studies of the delta wing case[2,3,7] were revealed by the nonlinear solutions. The first consisted of the appearance of a local pressure maximum at the corner, and the second consisted of the displacement of the vortical singularity away from the corner and along the wedge surface. The validity of these results was, however, in doubt because of certain physically incorrect assumptions made in Refs. 5 and 6. In order to gain some insight on this question, an analytical and experimental study was undertaken in Ref. 8. This study showed that the pressure near the corner behaves like

$$p \sim \zeta^{4\pi/\Phi-2}$$

where ζ is the distance away from the corner and Φ is the external angle (Fig. 1). For external angles greater than 240 deg, the pressure gradient $\partial p/\partial\zeta$ is infinite at $\zeta=0$ and the pressure distribution exhibits a cusp at the corner. This pressure distribution was also shown to result in a displacement away from the corner of the vortical singularity. These theoretical predictions were later confirmed by numerical experiments in Ref. 9 for the case $\Omega=0$. In the present paper, a parametric study based on a variation of the angle Ω (and, consequently, the angle Φ) will clearly show the development of this pressure behavior. In addition, a parametric study showing the effect of rounding the corner on the location of the vortical singularity is presented.

II. Numerical Formulation

The numerical solution to this problem begins by casting the time-dependent Euler equations in terms of spherical polar coordinates, such that t is time, r is the distance from the conical origin 0, in Fig. 1, θ is the polar angle measured from the z axis, and ϕ is the azimuthal angle measured counterclockwise from the x, y, z plane. Advantage is then taken of the conical nature of the problem by looking for the solution only on the surface of the unit sphere, $r=1$. The region of interest on the unit sphere is the region inside the Mach conoid emanating from the apex (Ref. 8); this region is shown on Fig. 3, after projection onto a y,x plane. The four boundaries of the region are: the wedge surface defined by

$$\theta_w(\phi) = \text{atan}\left[\frac{\tan\delta}{\sin\phi - \tan\Lambda\tan\delta\cos\phi}\right] \quad (1)$$

Presented as Paper 79-1511 at the AIAA 12th Fluid and Plasma Dynamics Conference, Williamsburg, Va., July 23-25, 1979; submitted Aug. 2, 1979; revision received Nov. 30, 1979.

Index categories: Computational Methods; Supersonic and Hypersonic Flow; Transonic Flow.

*Aerospace Technologist, Supersonic Aerodynamics Branch, High-Speed Aerodynamics Division. Member AIAA.

†A study of the asymmetric flow case will be published at a later date.

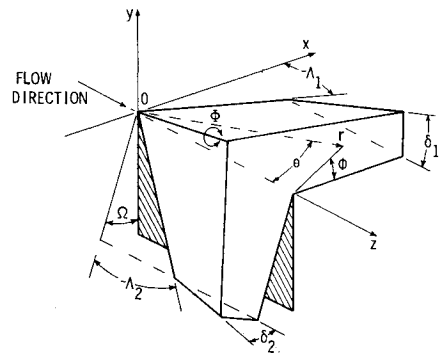

Fig. 1 Corner configuration.

the symmetry plane defined by

$$\phi_s = \tfrac{1}{2}(3/2\pi - \Omega) \tag{2}$$

the bow shock wave defined by

$$\theta = \theta_{sk}(\phi, t) \tag{3}$$

which is an unknown function that must be obtained as part of the solution to the problem, and the cross flow sonic line $\phi = \phi_{sl}(\theta)$, which is given implicitly by the relation

$$1 - \left(\frac{U_2}{a_2}\sin\phi + \frac{V_2}{a_2}\cos\phi\right)^2 - \left[\left(\frac{V_2}{a_2}\sin\phi - \frac{U_2}{a_2}\cos\phi\right)\cos\theta - \frac{W_2}{a_2}\sin\theta\right]^2 = 0 \tag{4}$$

The constants U_2, V_2, W_2 are the velocity components in the x, y, z directions, respectively, in the region behind the two-dimensional shock outboard of the cross flow sonic line, and a_2 is the speed of sound in the same region.

The cross flow sonic line is replaced, at least in part, by a cross flow shock if the leading edges are swept forward.[10] The disturbed region of the flow is then somewhat larger than the region bounded by the Mach conoid, and the location of the right-hand boundary must also be obtained as part of the solution. No attempt has been made in the present study to properly fit the cross flow shock as a discontinuity; however, for a number of swept forward configurations, the code has been capable of capturing the cross flow shock, producing results which appear qualitatively good.

In order to obtain a good distribution of grid points and avoid differentiating across the cross flow sonic line, where the first derivatives of some flow variables are multivalued,[10] new computational coordinates are defined by

$$X = \frac{\phi_s - \phi}{\phi_s - \phi_{sl}(Y)}, \quad Y = \frac{\theta - \theta_w(X)}{\theta_{sk}(X,T) - \theta_w(X)}, \quad T = t \tag{5}$$

such that the wedge surface, the symmetry plane, the bow shock, and the cross-flow sonic line are all mapped into grid lines. The transformation of partial derivatives from spherical independent variables to computational independent variables is obtained via the calculus of implicit functions.[11] An even distribution of grid points on the computational X, Y plane results in the distribution of grid points in the physical plane shown in Fig. 3.

After nondimensionalizing pressure, density, and temperature by their respective freestream values p_∞, ρ_∞, τ_∞, and velocity components by $\sqrt{p_\infty/\rho_\infty}$, the Euler equations in terms of computational X, Y, T coordinates are give by

$$Q_T + AQ_X + BQ_Y + H = 0 \tag{6}$$

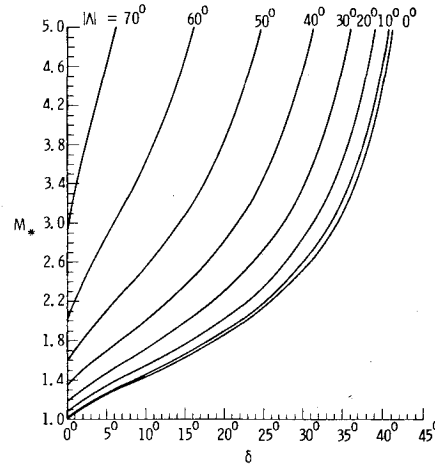

Fig. 2 Freestream limiting Mach number for shock detachment.

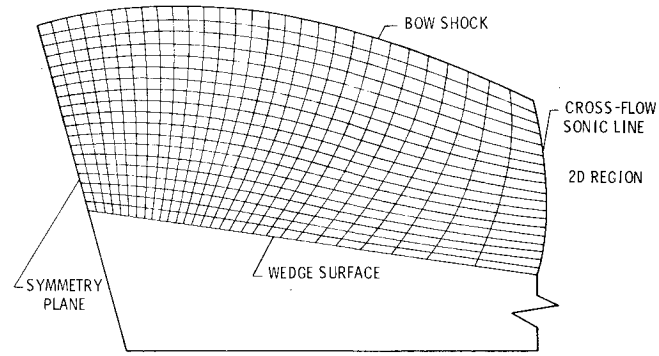

Fig. 3 Region of interest on unit sphere, projected onto the x,y plane, and typical grid lines.

$$Q = \begin{bmatrix} P \\ v \\ w \\ u \\ S \end{bmatrix} \tag{7}$$

where A, B, and H are defined in the Appendix. In the above equations, P is the natural logarithm of pressure, v, w, u, are the spherical velocity components in the positive θ, ϕ, and r directions, and S is the entropy which for an ideal gas is related to the pressure and temperature by

$$\tau = \exp\left(\frac{\gamma - 1}{\gamma}P + \frac{S}{\gamma}\right) \tag{8}$$

where γ is the adiabatic exponent.

Starting with a judiciously chosen set of initial conditions, the equations of motion, defined by Eq. (6), are integrated in time at all interior points using the MacCormack finite difference scheme[12] until a steady state is reached. Two modifications to this standard procedure were made during the development of the code. First, the integration of the entropy equation was perfomed using windward differences only.[13] This modification automatically resolves problems associated with the computation of the vortical singularity, and is more consistent with the physics than a straightforward application of the MacCormack scheme for this equation. Secondly, the radial momentum equation was replaced by Bernoulli's equation

$$u = \left(q_{\max}^2 - v^2 - w^2 - \frac{2\gamma}{\gamma - 1}\tau\right)^{1/2} \tag{9}$$

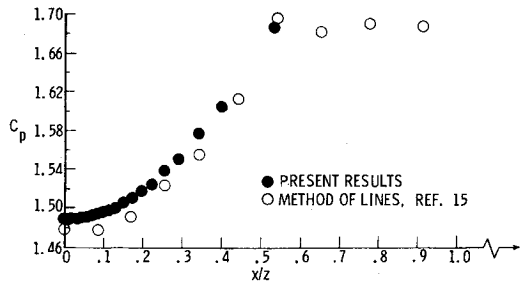

Fig. 4 Calculated pressure coefficient on wedge surface for $\Omega = 90$ deg, $\Lambda = -20$ deg, $\delta = 10$ deg, and $M_\infty = 3$.

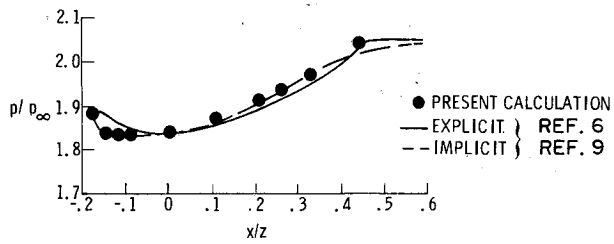

Fig. 5 Surface pressure for $\Omega = 0$ deg, $\Lambda = 0$ deg, $\delta = 10$ deg, and $M_\infty = 3$.

where $q_{\max}$ is the maximum flow speed. This replacement is strictly valid only in the steady state; however, when applied during the transient it removed small wiggles in the radial velocity component which developed when the radial momentum equation was integrated.

III. Computation of Boundary Points

The calculation of grid points on the wedge surface proved particularly difficult because of the extremely large gradients that can occur at the corner. The best results were obtained by integrating the cross flow momentum equation

$$q_T + b(e_\theta v_X + e_\phi w_X) + \tau\left(e_\theta X_\theta + \frac{e_\phi X_\phi}{\sin\theta}\right)P_X + uq = 0 \quad (10)$$

where e_θ and e_ϕ are the direction cosines of the unit tangent to the wall

$$\hat{e} = e_\theta \hat{\theta} + e_\phi \hat{\phi} \quad (11)$$

q is the cross flow velocity component

$$q = V \cdot \hat{e} = e_\theta v + e_\phi w \quad (12)$$

and b is defined in the Appendix. Once q is evaluated at the new time level, using the MacCormack scheme, the boundary condition at the surface requires that the θ and ϕ velocity components be given by

$$v = e_\theta q, \quad w = e_\phi q \quad (13)$$

The pressure is evaluated by replacing the first expression obtained from Eq. (6) by

$$P_t + qP_s + \gamma(q_s + q\beta_n + 2u + v\cot\theta) = 0 \quad (14)$$

which is obtained from the continuity equation (written in terms of the natural logarithm of pressure) using the transformations

$$\frac{\partial}{\partial\theta} = \sin\beta\frac{\partial}{\partial s} + \cos\beta\frac{\partial}{\partial n}$$

$$\frac{1}{\sin\theta}\frac{\partial}{\partial\phi} = \cos\beta\frac{\partial}{\partial s} - \sin\beta\frac{\partial}{\partial n} \quad (15)$$

where s and n are coordinates tangent and normal to cross flow streamlines (Ref. 10), and β is given by

$$\tan\beta = \frac{v}{w} = \frac{1}{\sin\theta}\frac{\partial\theta_w}{\partial\phi} \quad (16)$$

Recasting Eq. (14) in terms of computational coordinates, we obtain

$$P_T + bP_X + \gamma\left[\left(e_\theta X_\theta + \frac{e_\phi X_\phi}{\sin\theta}\right)q_X + q\beta_n + 2u + v\cot\theta\right] = 0 \quad (17)$$

and

$$q\beta_n = \frac{q}{1+\tan^2\beta}\frac{\partial\tan\beta}{\partial X} + \left(e_\phi Y_\theta - \frac{e_\theta Y_\phi}{\sin\theta}\right)\cdot(e_\phi v_Y - e_\theta w_Y) \quad (18)$$

The evaluation of the entropy and radial velocity component follows the same procedures as for interior points.

At the corner itself, because it is a cross flow stagnation point, the entropy equation degenerates to the form

$$S_t = 0 \quad (19)$$

so that at this point special precautions must be taken. If the corner is a nodal point, then two values of entropy are defined at the corner (and, consequently, two values of temperature, and radial velocity component). One value is obtained by extrapolation from the neighboring grid point along the wedge surface and another from the neighboring grid point along the symmetry plane. If the corner is a saddle point, then only one value is necessary. This value depends on whether the streamline reaching the corner is the streamline along the wall or the streamline along the symmetry plane.

The shock computation basically follows the procedures described by Moretti in Ref. 14. This simply involves defining a shock speed W_s

$$W_s = \frac{\partial\theta_{sk}(X,T)}{\partial T}\bigg|_{X=\text{const}} \quad (20)$$

such that the shock velocity is given by

$$W_s = W_s\hat{Y}$$

where $\hat{Y}$ is the unit tangent to the Y computational coordinate. Then by differentiating with respect to time the Rankine-Hugoniot pressure jump across the shock, it is possible to obtain the following expression for the shock acceleration:

$$\frac{\partial W_s}{\partial T} = \left[\frac{\partial V_\infty}{\partial T}\hat{N}_s + V_\infty\frac{\partial\hat{N}_s}{\partial T} - W_s\left(\frac{\partial\hat{Y}}{\partial T}\hat{N}_s + \hat{Y}\frac{\partial\hat{N}_s}{\partial T}\right) - \frac{\sqrt{\gamma}\left(M_{\text{rel}}^2 + \frac{1-\gamma}{2\gamma}\right)P_T}{2M_{\text{rel}}}\right]\Big/(\hat{Y}\cdot\hat{N}_s) \quad (22)$$

where $\hat{N}_s$ is the unit normal to the shock, M_{rel} is the normal component of freestream Mach number relative to a frame moving with the shock

$$M_{\text{rel}} = \frac{(V_\infty - W_s)\cdot\hat{N}_s}{\sqrt{\gamma}} \quad (23)$$

and P_T is obtained from the first expression defined by Eq. (6) using one-sided differences for the derivatives. Integrating

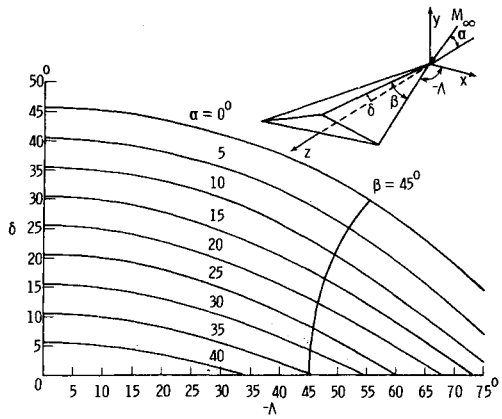

Fig. 6 Maximum angle of attack α for an attached shock corresponding to a given δ, Λ configuration with $\Omega = 90$ deg, $M_\infty = \infty$, and $\gamma = 7/5$.

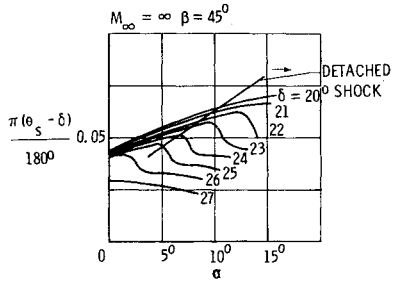

Fig. 7 Shock displacement in plane of symmetry after Gonor (Ref. 3).

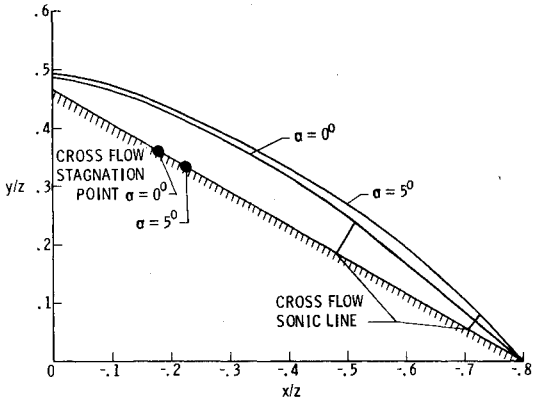

Fig. 8 Bow shock and cross flow stagnation points for a delta wing with $\beta = 45$ deg, $\delta = 25$ deg, and $M_\infty = 100$, at $\alpha = 0$ deg and 5 deg.

Eq. (22) twice yields the new shock position from which, through the Rankine-Hugoniot relations, the new values of the flow variables on the high pressure side of the shock are obtained.

The remaining two boundaries consist of the symmetry plane, which is evaluated in the same manner as the interior points with the additional constraint of symmetry, and the cross-flow sonic line boundary which is given by the known solution to the two-dimensional region.

IV. Results

Validation

The numerical code was validated by comparing its results with exact solutions and with the results of other numerical codes.

The comparison with the exact solution is obtained for the case where the leading edges are unswept and Ω corresponds to a right angle. This configuration results in a two-dimensional wedge. Although the analytic solution is trivial for this configuration, the numerical solution is far from

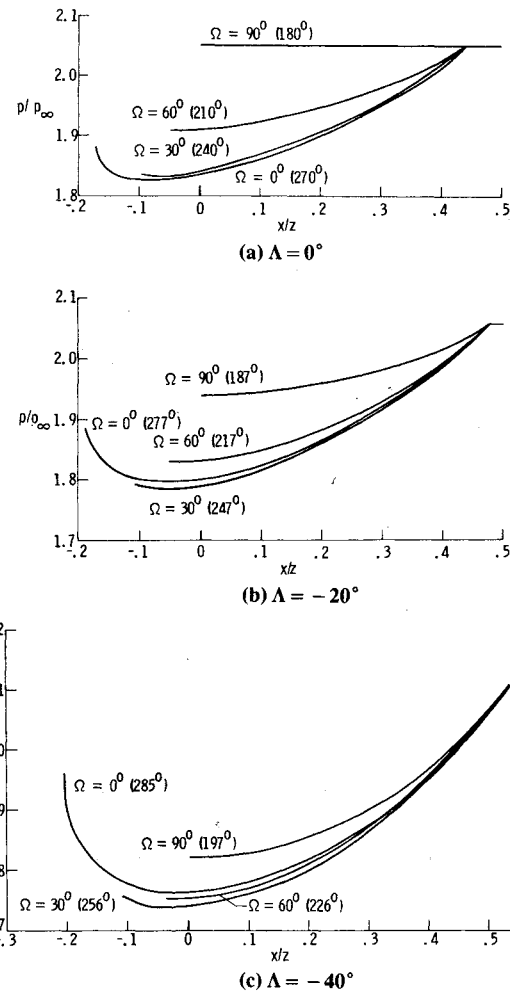

Fig. 9 Surface pressure distribution at $M_\infty = 3$ and $\delta = 10$ deg. External angle Φ in parentheses.

trivial because the velocity components being calculated are spherical components which are not constant. Several cases were computed typical of this configuration with resulting errors of less than 0.5% in any flowfield variable.

For a delta wing configuration corresponding to $\Omega = 90$ deg, $\Lambda = -20$ deg, $\delta = 10$ deg at freestream Mach number of 3 and adiabatic exponent of 7/5, a comparison was made with the "method of lines" described in Ref. 15. The computed pressure coefficient at the surface of the wedge is shown in Fig. 4. The discrepancy between the two methods is 0.8% at the corner, well within the accuracy of the numerical calculations.

For an unswept corner configuration corresponding to $\Omega = 0$ deg, $\Lambda = 0$ deg, $\delta = 10$ deg at freestream Mach number of 3 and adiabatic exponent of 7/5, a comparison was made against the numerical techniques reported in Refs. 6 and 9. The nondimensional surface pressure for this case is plotted on Fig. 5. The data for this comparison were kindly provided by Kutler and do not actually appear in Ref. 9. The present results agree very well with the implicit solution of Ref. 9, particularly near the corner. At the cross-flow sonic line there is some smearing of the sonic line by the implicit method. The poor results of the explicit method, Ref. 6, are apparently due to the improper boundary condition imposed at the corner.[8] The locations of both the vortical singularity and the bow shock wave predicted by all three calculation procedures are in good agreement for this case.

Anomalous Shock Behavior

For the delta wing configuration at high freestream Mach numbers, an analysis made by Gonor[2,3] using thin-shock-

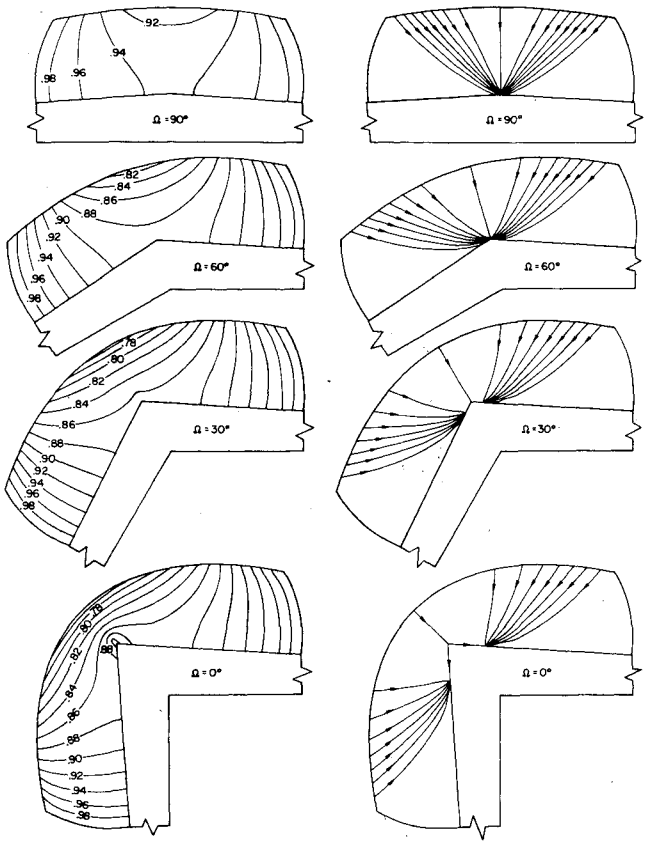

Fig. 10 Computed isobars and cross flow streamlines for $M_\infty = 3$ and $\Lambda = -20$ deg. Pressure levels are referred to pressure level in 2D region.

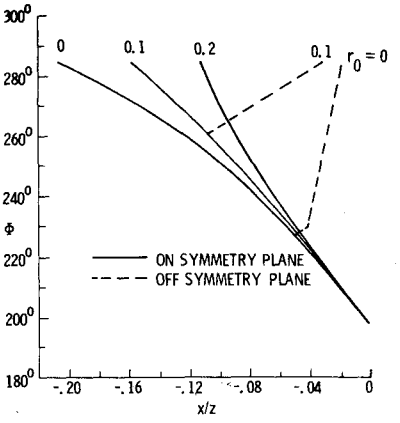

Fig. 11 Cross flow stagnation point location as a function of the external angle Φ and the corner radius r_0. $M_\infty = 3$, $\delta = 10$ deg, $\Lambda = -40$ deg.

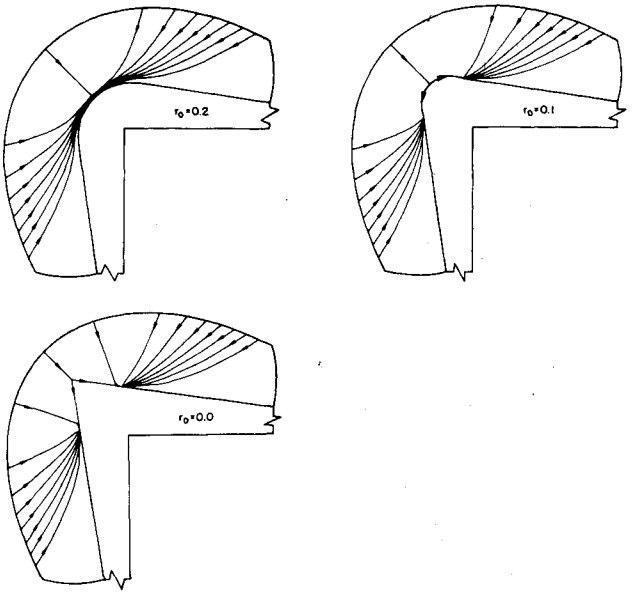

Fig. 12 Effect of corner radius on cross flow streamlines, $M_\infty = 3$, $\delta = 10$ deg, $\Lambda = -40$ deg, and $\Omega = 0$ deg.

layer theory predicts that at the plane of symmetry the distance between the shock and the surface of the wedge first increases as the angle of attack α of the freestream is increased, and then, beyond a certain angle of attack, an anomalous behavior occurs where the distance between the shock and the surface of the wedge begins to decrease. An attempt to duplicate numerically this interesting phenomenon indicated that the calculations made by Gonor were in error.

The apparent anomalous behavior predicted by Gonor comes about by continuing the solution he obtained, under the assumption of an attached leading-edge shock, beyond the point of shock detachment. This can be demonstrated by considering the following facts. The effective wedge angle δ_e is made up of a zero angle-of-attack contribution and an angle-of-attack contribution, and is given by

$$\delta_e = \text{atan}\left(\frac{\tan\delta}{\cos\Lambda}\right) + \text{atan}\left(\frac{\tan\alpha}{\cos\Lambda}\right) \tag{24}$$

This effective wedge angle must be less than the wedge detachment angle which at high freestream Mach numbers is given by

$$\delta_* = \text{asin}\,(1/\gamma) \tag{25}$$

The delta wing configurations studied by Gonor were defined in terms of the compression angle δ, ranging from 20 deg to 27 deg, and the angle β, defined as the angle on the surface of the wing between the leading edge and the corner. The angle β is related to Λ by

$$\Lambda = -\text{asin}(\cos\beta\sqrt{1+\tan^2\delta}) \tag{26}$$

In Fig. 6, the maximum angle of attack for an atttached shock for a given δ, Λ configuration at $M_\infty \to \infty$ is shown. From this figure we see that for $\beta = 45$ deg and $\delta = 20$ deg the effective wedge angle exceeds the detachment angle at $\alpha \sim 11$ deg, while for $\beta = 45$ deg and $\delta = 25$ deg, the detachment angle is exceeded at $\alpha \sim 6$ deg. If these results are superimposed on Fig. 12 of Ref. 3, we find that the anomalous shock behavior occurs for angles of attack corresponding to detached shocks as shown in Fig. 7.

In Fig. 8, the bow shock and cross flow stagnation point location for a delta wing of the type studied by Gonor ($\beta = 45$ deg, $\delta = 25$ deg) is shown at angles of attack of 0 deg and 5 deg for freestream Mach number of 100 and $\gamma = 7/5$. The 5 deg angle-of-attack case corresponds to a case where the shock is very close to the detachment point.

Parametric Studies

As mentioned in the introduction, a theoretical study in Ref. 8 indicated a singular behavior of the pressure at the corner for external angles Φ greater than 240 deg. A parametric study was conducted to investigate this phenomenon and the results are shown in Fig. 9. For all cases the compression angle δ was kept fixed at 10 deg and the freestream Mach number was set at 3, with $\gamma = 7/5$. Figure 9 shows the computed surface pressure for an unswept configuration with the angle Ω ranging between 90 and 0 deg. The $\Omega = 90$ deg case corresponds to a two-dimensional wedge with uniform pressure behind the oblique leading-edge shock. As the angle Ω is reduced, the pressure decreases at the corner until $\Omega = 30$ deg, corresponding to $\Phi \sim 240$ deg. Reduction of Ω

beyond this point causes an increase in the pressure at the corner with the cusp-like behavior predicted in Ref. 8. Figures 9b and 9c show similar results for leading-edge sweep of -20 and -40 deg, respectively. As indicated by the figures, the effect of sweeping the leading edges back is to reduce the pressure at the corner and to make more pronounced the cusp-like behavior at the corner for $\Phi > 240$ deg. It is evident from these results that corner loads can be minimized by sweeping the leading edges and by designing for external angles of approximately 240 deg.

In Fig. 10, the computed isobars and cross flow streamlines are shown for the cases corresponding to Fig. 9b ($\Lambda = -20$ deg). For $\Omega = 30$ deg and $\Omega = 0$ deg, the cross flow streamlines show the displacement of the vortical singularity away from the corner. A jump in density, temperature, and radial velocity component occurs at this nodal point.

A parametric study of the effect of the corner radius on the location of the cross flow stagnation point was carried out for the $\delta = 10$ deg and $\Lambda = -40$ deg configuration. The location of the cross flow stagnation point is plotted on Fig. 11 against the external angle Φ, which is more meaningful than the angle Ω. For the sharp corner $r_0 = 0$, the nodal point at the corner moves away from the corner, leaving behind a saddle point at $\Phi \sim 228$ deg, while at $r_0 = 0.2$ the corner remains a nodal point through the maximum Φ angle tested (corresponding to $\Omega = 0$ deg). These results are in qualitative agreement with those of Ref. 9. The cross-flow streamlines shown on Fig. 12 illustrate the effect of the corner radius.

V. Conclusion

A standard computational procedure has been applied to the calculation of external conical corners. Care has been taken in implementing the boundary conditions by fitting the bow shock wave and the cross-flow sonic line, constructing the computational mesh, formulating the governing equations, accounting for singularities, and in treating the body boundary condition. The numerical results obtained substantiate the theoretical structure developed in Ref. 8.

The anomalous shock behavior predicted by Gonor was shown to be the result of applying a theory beyond its range of application.

A parametric study based on the configuration defining angles showed how to design corners with minimum pressure loads.

Finally, it was shown that the vortical singularity can be maintained at the symmetry plane by rounding the corner.

Appendix

The matrices appearing in Eq. (6) are:

$$A = \begin{vmatrix} b & \gamma X_\theta & (\gamma X_\phi/\sin\theta) & 0 & 0 \\ \tau X_\theta & b & 0 & 0 & 0 \\ (\tau X_\phi/\sin\theta) & 0 & b & 0 & 0 \\ 0 & 0 & 0 & b & 0 \\ 0 & 0 & 0 & 0 & b \end{vmatrix} \quad \text{(A1)}$$

$$B = \begin{vmatrix} c & \gamma Y_\theta & (\gamma Y_\phi/\sin\theta) & 0 & 0 \\ \tau Y_\theta & c & 0 & 0 & 0 \\ (\tau Y_\phi/\sin\theta) & 0 & c & 0 & 0 \\ 0 & 0 & 0 & c & 0 \\ 0 & 0 & 0 & 0 & c \end{vmatrix} \quad \text{(A2)}$$

$$H = \begin{vmatrix} 2u + v\cot\theta \\ uv - w^2\cot\theta \\ -v^2 - w^2 \\ 0 \end{vmatrix} \quad \text{(A3)}$$

$$b = X_t + vX_\theta + (wX_\phi/\sin\theta)$$

$$c = Y_t + vY_\theta + (wY_\phi/\sin\theta) \quad \text{(A4)}$$

References

[1] Carafoli, E., *Wing Theory in Supersonic Flow*, 1st ed., Pergamon, London, 1969.

[2] Gonor, A. L. and Ostapenko, N. A., "Final Thickness Delta Wing in a Hypersonic Flow," *Fluid Dynamics Transactions*, edited by W. Fiszdon et al., Vol. 5, Pt. 2, 1971, pp. 83-95.

[3] Gonor, A. L., "Theory of Hypersonic Flow about a Wing," *Progress in Aerospace Sciences*, edited by D. Küchemann et al., Vol. 14, 1973, pp. 109-175.

[4] Vorob'ev, N. F., Fedosov, V. P., "Supersonic Flow Around a Dihedral Angle (Conical Case)," *Fluid Dynamics*, Vol. 7, No. 5, July 1974, pp. 852-856.

[5] Kutler, P., Shankar, V., Anderson, D. A., and Sorenson, R. L., "Internal and External Axial Corner Flow," *Aerodynamic Analysis Requiring Advanced Computers*, NASA SP-347, March, 1975, pp. 643-658.

[6] Kutler, P. and Shankar, V., "Computation of the Inviscid Supersonic Flow Over an External Axial Corner," *Proceedings of the 1976 Heat Transfer and Fluid Mechanics Institute*, Davis, Calif., June 1976, pp. 356-373.

[7] Oswatitsch, K., *Spezialgebiete der Gasdynamik*, Springer-Verlag, New York, 1977, pp. 202-203.

[8] Salas, M. D. and Daywitt, J., "Structure of the Conical Flowfield about External Axial Corners," *AIAA Journal*, Vol. 17, Jan. 1979, pp. 41-47.

[9] Kutler, P., Pulliam, T. H., and Vigneron, Y. C., "Computation of the Viscous Supersonic Flow over Symmetrical and Asymmetrical External Axial Corners," AIAA Paper 78-1135, July 1978.

[10] Salas, M. D., "Flow Patterns Near a Conical Sonic Line," *AIAA Journal*, Vol. 18, March 1980, pp. 227-234.

[11] Hildebrand, F. B., *Advanced Calculus for Applications*, Prentice-Hall, Englewood Cliffs, N.J., 1962, pp. 340-344.

[12] MacCormack, R. W., "The Effect of Viscosity in Hypervelocity Impact Cratering," AIAA Paper 69-354, April 1969.

[13] Moretti, G. and Pandolfi, M., "Analysis of the Inviscid Flow about a Yawed Cone—Preliminary Studies," Polytechnic Institute of Brooklyn, PIBAL Rept. 72-18, May 1972.

[14] Moretti, G., "Thoughts and Afterthoughts about Shock Computations," Polytechnic Institute of Brooklyn, PIBAL Rept. 72-37, Dec. 1972, pp. 39-42.

[15] Klunker, E. B., South, J. C., and Davis, R. M., "Calculation of Nonlinear Conical Flows by the Method of Lines," NASA TR R-374, Oct. 1971.